Materials for Renewable and Sustainable Energy (2020) 9:4
https://doi.org/10.1007/s40243-020-0164-x

ORIGINAL PAPER

A DFT investigation of the mechanisms of CO_2 and CO methanation on Fe (111)

Caroline R. Kwawu[1] · Albert Aniagyei[2] · Richard Tia[1] · Evans Adei[1]

Received: 15 October 2019 / Accepted: 4 January 2020 / Published online: 10 January 2020

Abstract

Insight into the detailed mechanism of the Sabatier reaction on iron is essential for the design of cheap, environmentally benign, efficient and selective catalytic surfaces for CO_2 reduction. Earlier attempts to unravel the mechanism of CO_2 reduction on pure metals including inexpensive metals focused on Ni and Cu; however, the detailed mechanism of CO_2 reduction on iron is not yet known. We have, thus, explored with spin-polarized density functional theory calculations the relative stabilities of intermediates and kinetic barriers associated with methanation of CO_2 via the CO and non-CO pathways on the Fe (111) surface. Through the non-CO (formate) pathway, a dihydride CO_2 species (H_2CO_2), which decomposes to aldehyde (CHO), is further hydrogenated into methoxy, methanol and then methane. Through the CO pathway, it is observed that the CO species formed from dihydroxycarbene is not favorably decomposed into carbide (both thermodynamically and kinetically challenging) but CO undergoes associative hydrogenation to form CH_2OH which decomposes into CH_2, leading to methane formation. Our results show that the transformation of CO_2 to methane proceeds via the CO pathway, since the barriers leading to alkoxy transformation into methane are high via the non-CO pathway. Methanol formation is more favored via the non-CO pathway. Iron (111) shows selectivity towards CO methanation over CO_2 methanation due to differences in the rate-determining steps, i.e., 91.6 kJ mol^{-1} and 146.2 kJ mol^{-1}, respectively.

Keywords Spin-polarized DFT-GGA · CO_2 methanation · CO methanation · Methanol formation · Reaction mechanism

Introduction

Carbon dioxide (CO_2) is a cheap, non-toxic and abundant carbon-one (C1) source for chemical processes [1–7] and its transformations into fuel offer solutions to the problem of global warming as well as helping to meet the world's increasing energy needs [8].

The catalytic hydrogenation of CO_2 into methane (natural gas) by the Sabatier reaction is an important process as natural gas has a range of applications such as electricity generation by gas and steam turbines, heating of buildings and cooking [9, 10].

$$CO_2 + 4\,H_2 \rightarrow CH_4 + 2\,H_2O\ \Delta H_{298K} = -252.9\ \text{kJ mol}^{-1}.$$

Despite the simplicity of the reaction, CO_2 methanation mechanism appears quite difficult to establish as several different opinions have been expressed on the nature of intermediate compounds involved and the rate-determining step [7]. Generally, two mechanisms have been proposed for CO_2 methanation, i.e., by the associative mechanism (non-CO pathway) or by the decomposition mechanism, where there is CO_2 direct dissociation into CO prior to methane formation, with the further reduction of CO through the CO methanation pathway [11–14]. Also for CO methanation, there is no consensus for the mechanism, whether by the alkoxy (CH_xO) intermediate or the CO decomposed carbide intermediate [7].

Late 3*d* metals, i.e., Fe, Ni, Cu, Co and Zn are metals thought to be responsible for CO_2 reduction in nature [15–19]. These transition metals in iron sulfide clusters are thought to provide the needed electrons for the reduction

Electronic supplementary material The online version of this article (https://doi.org/10.1007/s40243-020-0164-x) contains supplementary material, which is available to authorized users.

✉ Caroline R. Kwawu
kwawucaroline@gmail.com

[1] Department of Chemistry, Kwame Nkrumah University of Science and Technology, Kumasi, Ghana

[2] Department of Basic Sciences, University of Health and Allied Sciences, Ho, Ghana

process in the pre-biotic processes leading to the onset of life at the deep sea vents [18, 19], whereby CO_2 was converted into diverse organic molecules under reducing conditions at ambient temperature and pressure. Although Fe, Co, Ni, Cu and Zn surfaces have been identified for CO_2 activation and reduction experimentally, the reaction mechanism to producing hydrocarbons like methane is still not well understood on these surfaces [20, 21] and the earlier hydrogenation mechanism studies have focused mainly on Cu [22] and Ni surfaces [11–13, 23–27].

On clean Ni surfaces, most of these results supported the decomposition mechanism. Bartholomew and Weatherbee [11] earlier on in 1982 had studied CO_2 hydrogenation on Ni and reported CO_2 dissociation to CO. Peebles and Goodman [12] later experimentally studied CO_2 methanation on the Ni (100) surface and reported CO and C intermediates leading to CH_4 formation. Marwood et al. [13] submitted that the formate species is a spectator and CO is the key intermediate to methane formation. On the other hand, other studies supported the formate pathway. For example, Fujita et al. [24] observed that the kinetics of CO_2 and CO were different during the methanation process. The amount of carbide (C) on Ni was lower for CO_2 methanation than that in the CO methanation reaction, and hence inferred that CO_2 and CO methanation occurred via different pathways. Schild et al. [28] reported the formate intermediate and pathway on nickel. Formate and other compounds like carbonates, formaldehyde, methylate and methanol were observed on copper and palladium in the hydrogenation of CO_2 and CO, where formate was the primary compound reduced to methane on both surfaces [29].

With the spin-polarized density functional theory with a generalized gradient approximation (DFT-GGA) exchange–correlation functional, the complete hydrogenation reaction pathways of CO_2 reduction to methane have been explored on Cu (211) [22] and Ni (110) [27] surfaces. It was found on Cu (211) that methane formation was preferred through the CO pathway via the carboxylate intermediate. However, the studies on Ni (110) revealed that the methane formation via hydroxycarbene intermediate requires a lower energy barrier than via carbon monoxide and formate intermediates. The mechanism of CO_2 methanation has been underexplored on iron; we have investigated both the kinetics and thermodynamics of CO_2 and CO methanation on Fe (111) surface.

Computational details

All geometry optimizations and total energy calculations were carried out using the spin-polarized density functional theory generalized gradient approximation (DFT-GGA) method. The plane-wave basis sets and ultra-soft pseudopotentials were employed within the Quantum ESPRESSO Package [30], which performs full self-consistent DFT calculations to solve the Kohn–Sham equations [31]. The Perdew, Burke, Ernzerhof (PBE) [32] GGA exchange–correlation functional was employed. The Fermi-surface effects were treated by the smearing technique of Fermi–Dirac, using a smearing parameter of 0.003 Ry. An energy convergence threshold defining self-consistency of the electron density was set to 10^{-6} eV and a beta defining mixing factor for self-consistency of 0.2 was used. The Grimme-D2 Van der Waals correction was employed in all calculations. The graphics of the atomic structures and the iso-surfaces of the differential electron density plots in this manuscript have been prepared with the XCrysDen software [33].

The surface was created from the optimized bulk using the METADISE code [34]. Surfaces were described with the slab model, where periodic boundary conditions are applied to the central super-cell, so that it is reproduced periodically throughout space [35]. A vacuum region of 12 Å perpendicular to each surface was tested to be sufficient to avoid interactions between periodic slabs. An energy cut-off of 40 Ry (544 eV) and charge density cut-off of 320 Ry (4354 eV) were employed for the expansion of the plane-wave basis set. This is sufficient to converge the total energy of the iron systems and the Brillion zone was sampled using $(9\times9\times9)$ and $(3\times5\times1)$ Monkhorst–Pack [36] k-points mesh for the bulk and $p(3\times2)$ surface, respectively. Each slab is made up of the 36 atoms whereby there are 6 layers and 6 atoms in each layer. In all calculations, the top 3 layers and adsorbate are allowed to relax and bottom 3 layers fixed to mimic the bulk material as employed in earlier computations [37, 38]. The Climbing Image Nudged Elastic Band (CI-NEB) method was used to determine all transition-state structures along the reaction coordinate. The importance of zero-point energy correction has been checked for smaller models and found to follow the same trend.

Results and discussion

Reaction energies for CO_2 hydrogenation

To explore the intermediates involved in the hydrogen-assisted CO_2 and CO methanation on the Fe (111) surface, several starting geometries were optimized by the stepwise hydrogen addition to CO_2 and CO, which were optimized to obtain stable conformations (see Figure S1 of the supporting information file). The inter-atomic distances of the structures in Figure S1 are reported in Table S1 of the supporting information file. Upon obtaining all the optimized ground-state structures, the transition-state structures were sought for along two possible pathways, i.e., the non-CO

pathway through the formate intermediate and the CO pathway through the carboxylate intermediate. Series of elementary steps were considered within each of the two reaction pathways and a systematic representation is illustrated in Figs. 1, 2 and Table 1.

The relative energies (ΔE) for the ground-state structures and the transition-state structures were calculated relative to the isolated slab, $CO_{2(g)}$ and $x½\ H_{2(g)}$, using the formula shown below;

$$\Delta E = E_{(\text{final})} - E_{(\text{initial})},$$

where $E_{(\text{final})}$ is the energy of the ground-state or transition-state structure and $E_{(\text{initial})}$ is the energy of the gas-phase starting materials.

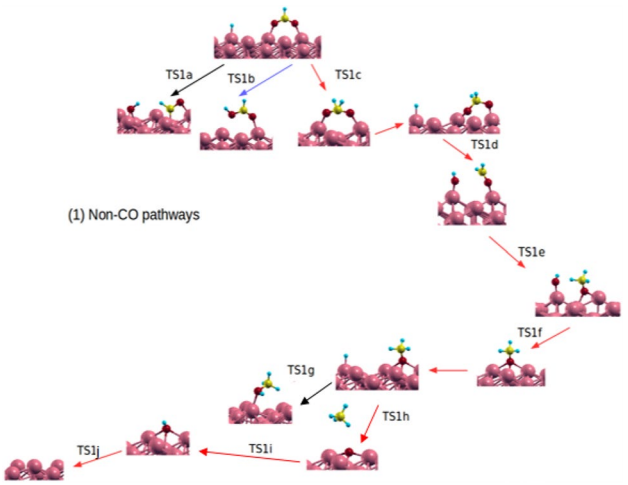

Fig. 1 A schematic representation of the possible transformations via the non-CO pathway

CO_2 adsorption on Fe (111) is seen to require an energy barrier of − 4.6 kJ mol^{-1} [38]. In this study, hydrogenation of the Fe (111) surface is also seen to be barrier less and dissociative; hence, atomic hydrogen co-adsorption is explored in each elementary step via the Langmuir–Hinshelwood-type reaction. As shown in Fig. 3, along the non-CO path, formate formed from CO_2 hydrogenation (reaction barrier = 0.1 kJ mol^{-1}) could be hydrogenated into CHO and OH (via TS1a), formic acid (via TS1b) or dihydride-CO_2 species (via TS1c). It is seen that formate goes through the highest barrier to form decomposed species (CHO+OH) (barrier = 271.1 kJ mol^{-1}). Formate transformation into formic acid is more favorable (barrier = 120.6 kJ mol^{-1}); however, a much lower kinetic barrier is seen for the production of the dihydride-CO_2 species, i.e., H_2CO_2 (65.9 kJ mol^{-1}). H_2CO_2 is transformed into aldehyde (CHO) upon further hydrogenation (barrier = 98.4 kJ mol^{-1}). Although the formation of the aldehyde is thermodynamically and kinetically challenging, the further hydrogenation of the aldehyde through TS1e requires a moderate barrier of 20.6 kJ mol^{-1} to produce a stable methoxy species of energy − 198.4 kJ mol^{-1}. Methanation of methoxy is very challenging requiring an energy barrier of 186.5 kJ mol^{-1} and thus making it a very slow process which might not be realized. However, methanol formation requires a lower barrier of 115.6 kJ mol^{-1}. Kinetically, the methanation of CO_2 via the non-CO pathway will selectively proceed via the following intermediates; formate, dihydride-CO_2, aldehyde and methoxy. Methanol formation is more favored kinetically through this pathway, with the rate-limiting step for formic acid, methanol, methane formation to be 127.6 kJ mol^{-1}, 115.6 kJ mol^{-1} and 186.5 kJ mol^{-1}, respectively.

Along the CO pathways, CO_2 hydrogenation into carboxylate requires an energy barrier of 96 kJ mol^{-1} (see

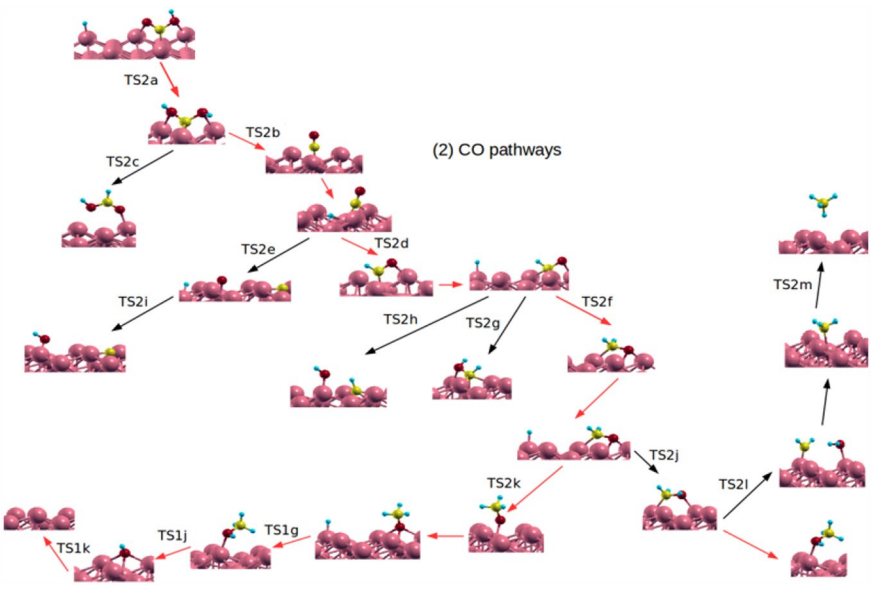

Fig. 2 A schematic representation of the possible pathways via the CO pathway

Table 1 Elementary steps, illustrations as seen in reaction schemes (Figs. 1, 2) for the transformation of CO_2 via the non-CO and CO pathways

Reactants	Transition States	Products
HCOO* + H*	TS1a	HCO* + OH*
HCOO* + H*	TS1b	HCOOH*
HCOO* + H*	TS1c	H_2CO_2*
H_2CO_2* + H*	TS1d	H_2CO* + OH*
H_2CO* + H* + OH*	TS1e	H_3CO* + OH*
H_3CO* + H* + OH*	TS1f	H_3CO* + H_2O
H_3CO* + H* + H_2O	TS1g	CH_3OH* + H_2O
H_3CO* + H* + H_2O	TS1h	CH_4 + O* + H_2O
CH_4 + O* + H* + H_2O	TS1i	CH_4 + OH* + H_2O
CH_4 + OH* + H* + H_2O	TS1j	CH_4 + 2 H_2O
COOH* + H*	TS2a	HOCOH*
HOCOH*	TS2b	CO* + H_2O
HOCOH*	TS2c	HCOOH*
CO* + H* + H_2O	TS2d	HCO* + H_2O
CO* + H* + H_2O	TS2e	C* + O* + H* + H_2O
HCO* + H* + H_2O	TS2f	H_2CO* + H_2O
HCO* + H* + H_2O	TS2g	HCOH* + H_2O
HCO* + H* + H_2O	TS2h	CH* + OH* + H_2O
C* + O* + H* + H_2O	TS2i	CH* + O* + H_2O
H_2CO* + H* + H_2O	TS2j	CH_2OH* + H_2O
H_2CO* + H* + H_2O	TS2k	CH_3O* + H_2O
CH_2OH* + H* + H_2O	TS2l	CH_2* + 2 H_2O
CH_3* + H* + 2 H_2O	TS2m	CH_4 + 2 H_2O

*Adsorbed species

Fig. 4). Carboxylate hydrogenation leads to dihydroxycarbene formation with a barrier of 146.2 kJ mol^{-1}. Dihydroxycarbene, being an unstable intermediate, once formed prefers to decompose into CO (TS2b = 28.9 kJ mol^{-1}) than to rearrange into formic acid (TS2c = 156.2 kJ mol^{-1}). The further decomposition of CO into carbide is seen to be both kinetically and thermodynamically challenging through TS2e, (with an energy barrier of 137.2 kJ mol^{-1}) implying the carbide formation is unlikely to occur. CO would rather produce HCO requiring an energy barrier of 91.6 kJ mol^{-1}. Further hydrogenation of HCO could lead to the formation of three possible intermediates, a decomposed CH + hydroxyl intermediate (with the highest barrier i.e. 191.8 kJ mol^{-1}), an alcohol group (barrier of 114.3 kJ mol^{-1}) or the alkoxy group (which has the least energy barrier i.e. 55.9 kJ mol^{-1}). Therefore, the carbon center of HCO is further hydrogenated to form H_2CO. H_2CO could further be hydrogenated into H_3CO (TS2j = 4.5 kJ mol^{-1}) or CH_2OH (TS2k = 28.8 kJ mol^{-1}). CH_2OH is preferred and decomposes into CH_2 through a barrier of 65.4 kJ mol^{-1} (TS2l). CH_2 is then protonated into CH_3 and methane. Kinetically via the CO pathway, CO_2 selectively converts into methane through the carboxylate, dihydroxycarbene, CO, alkoxy and alkyl intermediates. The slowest step for formic acid, CO, methanol and methane formation via the CO pathway involves the energy barriers, 156.2 kJ mol^{-1}, 146.2 kJ mol^{-1}, 146.2 kJ mol^{-1}, 146.2 kJ mol^{-1}, respectively.

Comparing the rate-limiting step leading to the formation of the desired products, i.e. CO, formic acid, methanol and methane along both the CO and non-CO pathways, the preferred pathway leading to the formation of these products can be determined. Of the two pathways explored (CO and non-CO pathways), the one providing the least rate-limiting step indicates selectivity and is the preferred pathway. Formic acid is preferentially produced via the non-CO pathway through the following intermediates: CO_2 and formate intermediates, with the rate-determining step being the hydrogenation of formate into formic acid (127.6 kJ mol^{-1}). Methanol production from CO_2 is favored via the non-CO pathway as well as through the following intermediates: CO_2, formate, dihydride-CO_2, CH_2O and methoxy intermediates, with rate-determining step being the hydrogenation of methoxy to methanol (115.6 kJ mol^{-1}). Methanol will be selectively

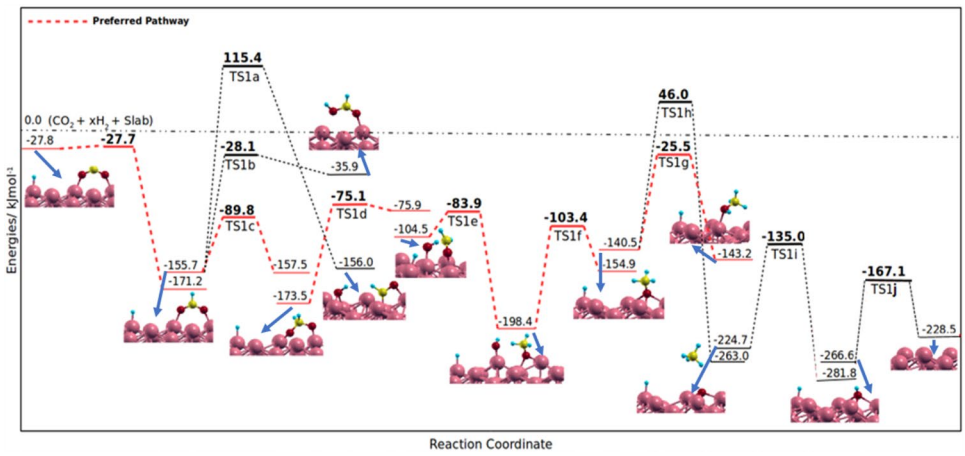

Fig. 3 Energy profile diagram along the non-CO pathway

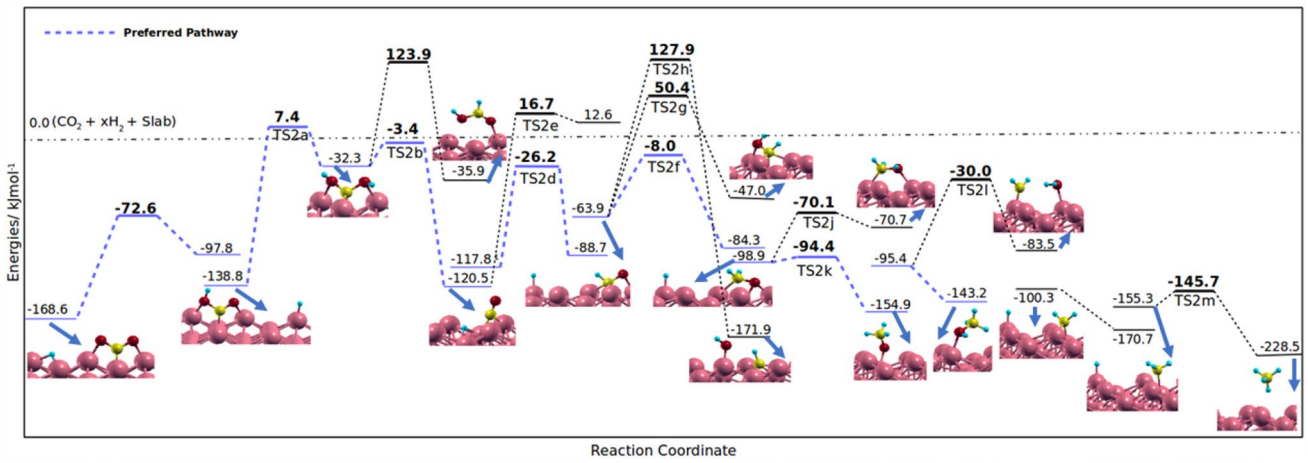

Fig. 4 Energy profile diagram along the CO pathway

produced from CO (over CO_2) via the following intermediates: carboxylate, dihydroxycarbene, CO, HCO, CH_2O and methoxy intermediates. The slowest step is the hydrogenation of CO into HCO (91.6 kJ mol^{-1}).

Methane and CO formation will occur via the carbonyl pathway; methane formation will proceed through the following intermediates: carboxylate, dihydroxycarbene, CO, HCO, H_2CO, H_2COH, CH_2 and CH_3. The slowest step for both the methanation and CO formation process involves carboxylate hydrogenation into dihydroxycarbene (146.2 kJ mol^{-1}). CO methanation is more favorable on Fe (111) over CO_2 methanation, occurring via the intermediates HCO, H_2CO, H_2COH, CH_2 and CH_3. CO methanation proceeds with the slowest step involving CO hydrogenation into HCO (91.6 kJ mol^{-1}), as seen earlier for methanol production from CO. CO hydrogenation controls both the rate of methanol and methane formation from CO; hence, these reactions are very competitive for CO reduction on Fe (111) and lowering the barrier for CO protonation is desirable to speed up both processes. Formate hydrogenation, methoxy hydrogenation and carboxylate hydrogen-assisted transformation into CO control the rate of CO_2 transformation to formic acid, methanol and methane, respectively. Thus, modified Fe (111) surfaces enhancing these reaction steps have the potential to improve the CO_2 conversion processes.

Our results show that CO_2 methanation on Fe (111) occurs via the CO pathway through the following transformations: carboxylate protonation to dihydroxycarbene (HOCOH), decomposition to carbon monoxide (CO), protonation of CO to HCO, protonation to H_2CO to alkoxy, protonation on alkoxy (CH_2–OH) and water production, leading to CH_2 and CH_3 formation. CO_2 methanation on Cu (211) using the computational hydrogen electrode is seen to proceed via the CO and carboxylate intermediates as well [22]. Also, on the Ni (110) surface, dihydroxycarbene, CO and CH_2OH are reported to be intermediates leading to methane production, with water removal from the surface been the rate limiting step [27]. The mechanism of CO_2 methanation on Ni (100) shows that large amount of CO is formed over methane as activation energies of 88.7 and 72.8–82.4 kJ/mol are observed for methane and CO production, respectively. However, on Fe (111), the activation energies for CO formation and methanation are same, i.e., 146.2 kJ mol^{-1} [12]. Again, Fe (111) does not favor the carbide pathway as reported on Ni (100). Cu is also seen to reduce CO_2 via the carboxylate, CO, HCO and methoxy intermediates; while the reaction barriers were not considered [22].

Conclusion

Our spin polarized-D2-GGA-DFT calculations reveal that CO_2 methanation will occur via the CO pathway and not the non-CO pathway. Fe (111) selectively favors CO methanation over CO_2 methanation, since although the reaction pathways are similar, the highest energy barrier for CO_2 methanation is encountered during the hydrogen-assisted CO_2 transformation into CO via the carboxylate and dihydroxycarbene intermediates. Both the formation of formic acid and methanol will proceed via the non-CO pathway, while CO and methane will be formed via the CO pathway from CO_2. CO_2 methanation on Fe (111) will involve the initial sequential hydrogenation of CO_2 into carboxylate, dihydroxycarbene, CO, HCO, H_2CO, and CH_2OH. CH_2OH is then decomposed into CH_2 and protonated into CH_3 and methane. Altering the rate-determining steps on modified Fe (111) surface is promising for CO_2 transformation and valorization.

Acknowledgements CRK is grateful for the Grants from The World Academy of Sciences (TWAS) and Swedish International Development Cooperation Agency (SIDA). CRK and RT acknowledge the UK's Royal Society and Leverhulme Trust for a research Grant under the Royal Society-Leverhulme Africa Postdoctoral Fellowship Award Scheme. Authors acknowledge the Center for High Performance Computing (CHPC), South Africa for additional computing resources.

References

1. Sakakura, T., Choi, J.-C., Yasuda, H.: Transformation of carbon dioxide. Chem. Rev. **107**, 2365–2387 (2007). https://doi.org/10.1021/cr068357u
2. Arakawa, H., Aresta, M., Armor, J.N., Barteau, M.A., Beckman, E.J., Bell, A.T., Bercaw, J.E., Creutz, C., Dinjus, E., Dixon, D.A., Domen, K., DuBois, D.L., Eckert, J., Fujita, E., Gibson, D.H., Goddard, W.A., Goodman, D.W., Keller, J., Kubas, G.J., Kung, H.H., Lyons, J.E., Manzer, L.E., Marks, T.J., Morokuma, K., Nicholas, K.M., Periana, R., Que, L., Rostrup-Nielson, J., Sachtler, W.M., Schmidt, L.D., Sen, A., Somorjai, G.A., Stair, P.C., Stults, B.R., Tumas, W.: Catalysis research of relevance to carbon management: progress, challenges, and opportunities. Chem. Rev. **101**, 953–996 (2001). https://doi.org/10.1021/cr000018s
3. Ma, J., Sun, N., Zhang, X., Zhao, N., Xiao, F., Wei, W., Sun, Y.: A short review of catalysis for CO_2 conversion. Catal. Today **148**, 221–231 (2009). https://doi.org/10.1016/j.cattod.2009.08.015
4. Talmage, S.C., Gobler, C.J.: Effects of past, present, and future ocean carbon dioxide concentrations on the growth and survival of larval shellfish. Proc. Natl. Acad. Sci. USA **107**, 17246–17251 (2010). https://doi.org/10.1073/pnas.0913804107
5. Song, C.: Global challenges and strategies for control, conversion and utilization of CO_2 for sustainable development involving energy, catalysis, adsorption and chemical processing. Catal. Today **115**, 2–32 (2006). https://doi.org/10.1016/j.cattod.2006.02.029
6. Centi, G., Perathoner, S.: Opportunities and prospects in the chemical recycling of carbon dioxide to fuels. Catal. Today **148**, 191–205 (2009). https://doi.org/10.1016/j.cattod.2009.07.075
7. Wang, W., Wang, S., Ma, X., Gong, J.: Recent advances in catalytic hydrogenation of carbon dioxide. Chem. Soc. Rev. **40**, 3703–3727 (2011). https://doi.org/10.1039/c1cs15008a
8. Jiang, Z., Xiao, T., Kuznetsov, V.L., Edwards, P.P.: Turning carbon dioxide into fuel. Philos. Trans. A. Math. Phys. Eng. Sci. **368**, 3343–3364 (2010). https://doi.org/10.1098/rsta.2010.0119
9. Wei, W., Jinlong, G.: Methanation of carbon dioxide: an overview. Front. Chem. Sci. Eng. **5**, 2–10 (2010). https://doi.org/10.1007/s11705-010-0528-3
10. Wang, W., Su, C., Wu, Y., Ran, R., Shao, Z.: Progress in solid oxide fuel cells with nickel-based anodes operating on methane and related fuels. Chem. Rev. **113**, 8104–8151 (2013). https://doi.org/10.1021/cr300491e
11. Weatherbee, G.D., Bartholomew, C.H.: hydrogenation of CO_2 on Group viii metals. J. Catal. **77**, 460–472 (1982). https://doi.org/10.1016/0021-9517(82)90186-5
12. Peebles, D.E., Goodman, D.W., White, J.M.: Methanation of carbon dioxide on nickel(100) and the effects of surface modifiers. J. Phys. Chem. **87**, 4378–4387 (1983). https://doi.org/10.1021/j100245a014
13. Marwood, M., Doepper, R., Renken, A.: In-situ surface and gas phase analysis for kinetic studies under transient conditions: the catalytic hydrogenation of CO_2. Appl. Catal. A Gen. **151**, 223–246 (1997). https://doi.org/10.1016/S0926-860X(96)00267-0
14. Schild, C., Wokaun, A.: On the mechanism of CO and CO_2 hydrogenation reactions on zirconia-supported catalysts: a difkse reflectance FTIR study Part II: Surface species on copper/zirconia catalysts: implications for methanol synthesis selectivity. J Mol Catal **63**, 243–254 (1990). https://doi.org/10.1016/0304-5102(90)85147-A
15. Shin, W., Lee, S.H., Shin, J.W., Lee, S.P., Kim, Y.: Highly selective electrocatalytic conversion of CO_2 to CO at – 0.57 V (NHE) by carbon monoxide dehydrogenase from *Moorella thermoacetica*. J. Am. Chem. Soc. **125**, 14688–14689 (2003). https://doi.org/10.1021/ja037370i
16. Jeoung, J.-H., Dobbek, H.: Carbon dioxide activation at the Ni, Fe-cluster of anaerobic carbon monoxide dehydrogenase. Science **318**, 1461–1464 (2007). https://doi.org/10.1126/science.1148481
17. Gong, W., Hao, B., Wei, Z., Ferguson, D.J., Tallant, T., Krzycki, J.A., Chan, M.K.: Structure of the alpha2epsilon2 Ni-dependent CO dehydrogenase component of the *Methanosarcina barkeri* acetyl-CoA decarbonylase/synthase complex. Proc. Natl. Acad. Sci. USA **105**, 9558–9563 (2008). https://doi.org/10.1073/pnas.0800415105
18. Wächtershäuser, G.: Groundworks for an evolutionary biochemistry: the iron-sulphur world. Prog. Biophys. Mol. Biol. **58**, 85–201 (1992). https://doi.org/10.1016/0079-6107(92)90022-X
19. Saito, M.A., Sigman, D.M., Morel, F.M.: The bioinorganic chemistry of the ancient ocean: the co-evolution of cyanobacterial metal requirements and biogeochemical cycles at the Archean–Proterozoic boundary? Inorgan. Chim. Acta. **356**, 308–318 (2003). https://doi.org/10.1016/S0020-1693(03)00442-0
20. Solymosi, F.: The bonding, structure and reactions and promoted metal surfaces of CO_2 adsorbed on clean. J. Mol. Catal. **65**, 1 (1991). https://doi.org/10.1016/0304-5102(91)85070-I
21. Freund, H.-J., Roberts, M.W.: Surface chemistry of carbon dioxide. Surf. Sci. Rep. (1996). https://doi.org/10.1016/S0167-5729(96)00007-6
22. Peterson, A.A., Abild-Pedersen, F., Studt, F., Rossmeisl, J., Nørskov, J.K.: How copper catalyzes the electroreduction of carbon dioxide into hydrocarbon fuels. Energy Environ. Sci. **3**, 1311 (2010). https://doi.org/10.1039/c0ee00071j
23. Sehested, J., Larsen, K.E., Kustov, A.L., Frey, A.M., Johannessen, T., Bligaard, T., Andersson, M.P., Nørskov, J.K., Christensen, C.H.: Discovery of technical methanation catalysts based on computational screening. Top. Catal. (2007). https://doi.org/10.1007/s11244-007-0232-9
24. Fujita, S., Terunuma, H., Nakamura, M., Takezawa, N.: Mechanisms of methanation of carbon monoxide and carbon dioxide over nickel. Ind. Eng. Chem. Res. **30**, 1146–1151 (1991). https://doi.org/10.1021/ie00054a012
25. Magdysyuk, O.V., Adams, F., Liermann, H.-P., Spanopoulos, I., Trikalitis, P.N., Hirscher, M., Morris, R.E., Duncan, M.J., McCormick, L.J.: Dinnebier RE: Understanding the adsorption mechanism of noble gases Kr and Xe in CPO-27-Ni, CPO-27-Mg, and ZIF-8. Phys. Chem. Chem. Phys. **20**, 1–6 (2016). https://doi.org/10.1039/x0xx00000x

26. Sang, J.C., Hae, J.K., Kim, S.J., Park, S.B., Dong, H.P., Do, S.H.: Adsorbed carbon formation and carbon hydrogenation for CO_2 methanation on the Ni(111) surface: aSED-MO study. Bull. Korean Chem. Soc. **26**, 1682–1688 (2005). https://doi.org/10.5012/bkcs.2005.26.11.1682
27. Bothra, P., Periyasamy, G., Pati, S.K.: Methane formation from the hydrogenation of carbon dioxide on Ni(110) surface—a density functional theoretical study. Phys. Chem. Chem. Phys. **15**, 5701–5706 (2013). https://doi.org/10.1039/c3cp44495c
28. Schild, C., Wokaun, A., Koeppel, R.A., Baiker, A.: CO_2 hydrogenation over nickel/zirconia catalysts from amorphous precursors: on the mechanism of methane formation. J. Phys. Chem. (1991). https://doi.org/10.1021/j100169a049
29. Schild, C., Wokaun, A., Baiker, A.: On the hydrogenation of CO and CO_2 over copper/zirconia and palladium/zirconia catalysts. Fresenius J. Anal. Chem. (1991). https://doi.org/10.1007/BF00321943
30. Giannozzi, P., Baroni, S., Bonini, N., Calandra, M., Car, R., Cavazzoni, C., Ceresoli, D., Chiarotti, G.L., Cococcioni, M., Dabo, I., Dal Corso, A., de Gironcoli, S., Fabris, S., Fratesi, G., Gebauer, R., Gerstmann, U., Gougoussis, C., Kokalj, A., Lazzeri, M., Martin-Samos, L., Marzari, N., Mauri, F., Mazzarello, R., Paolini, S., Pasquarello, A., Paulatto, L., Sbraccia, C., Scandolo, S., Sclauzero, G., Seitsonen, A.P., Smogunov, A., Umari, P., Wentzcovitch, R.M.: QUANTUM ESPRESSO: a modular and open-source software project for quantum simulations of materials. J. Phys. Condens. Matter **21**, 395502 (2009). https://doi.org/10.1088/0953-8984/21/39/395502
31. Kohn, W., Sham, L.J.: Self-consistent equations including exchange and correlation effects. Phys. Rev. **20**, 140 (1965). https://doi.org/10.1103/PhysRev.140.A1133
32. Perdew, J., Burke, K., Ernzerhof, M.: Generalized gradient approximation made simple. Phys. Rev. Lett. **77**, 3865–3868 (1996). https://doi.org/10.1103/PhysRevLett.77.3865
33. Kokalj, A.: XCrySDen-A new program for displaying crystalline structures and electron densities. J. Mol. Graph. Model. **17**, 176–179 (1999). https://doi.org/10.1016/S1093-3263(99)00028-5
34. Watson, G.W., Kelsey, E.T., de Leeuw, N.H., Harris, D.J., Parker, S.C.: Atomistic simulation of dislocations, surfaces and interfaces in MgO. J. Chem. Soc. Faraday Trans. (1996). https://doi.org/10.1039/ft9969200433
35. Greeley, J., Nørskov, J.K., Mavrikakis, M.: Electronic structure and catalysis on metal surfaces. Annu. Rev. Phys. Chem. **53**, 319–348 (2002). https://doi.org/10.1146/annurev.physchem.53.100301.131630
36. Pack, J.D., Monkhorst, H.J.: "special points for Brillouin-zone integrations"—a reply. Phys. Rev. (1977). https://doi.org/10.1103/PhysRevB.16.1748
37. Kwawu, C.R., Tia, R., Adei, E., Dzade, N.Y., Catlow, C.R.A., Leeuw, N.H.De: Applied surface science effect of nickel monolayer deposition on the structural and electronic properties of the low miller indices of (BCC) iron: a DFT study. Appl. Surf. Sci. **400**, 293–303 (2017). https://doi.org/10.1016/j.apsusc.2016.12.187
38. Kwawu, C.R., Tia, R., Adei, E., Dzade, N.Y., Catlow, C.R.A., De Leeuw, N.H.: CO_2 activation and dissociation on the low miller index surfaces of pure and Ni-coated iron metal: a DFT study. Phys. Chem. Chem. Phys. **19**, 19478–19486 (2017). https://doi.org/10.1039/c7cp03466k